Article:

Nawaz, M, Heitor, A orcid.org/0000-0002-2346-8250 and Sivakumar, M (2023) Triaxial Stress-Strain Behavior of a Novel Basalt Rock Wasteand Ground Granulated Blast Furnace Slag Geopolymer. Journal of Materials in Civil Engineering, 35 (5). ISSN 0899-1561

https://doi.org/10.1061/(ASCE)MT.1943-5533.0004717

Triaxial stress-strain behaviour of a novel basalt rock waste and ground granulated blast furnace slag geopolymer

Mohsin Nawaz[1], Ana Heitor[2] and Muttucumaru Sivakumar[3]

[1]PhD Candidate, School of Civil, Mining and Environmental Engineering, University of Wollongong, Wollongong, NSW 2522, Australia (Corresponding author)

Email: mn291@uowmail.edu.au https://orcid.org/0000-0001-8953-3599

[2]Lecturer, School of Civil Engineeing, University of Leeds, Leeds, UK https://orcid.org/0000-0002-2346-8250

[3]Associate Professor, School of Civil, Mining and Environmental Engineering, University of Wollongong, Wollongong, NSW 2522, Australia

https://orcid.org/0000-0002-6315-7967

Abstract

Basalt rock waste is a major industrial waste generated as a result of quarrying of rocks and artificial sand manufacturing for construction projects and its disposal can lead to several landfill hazards. However, it shows potential to be used as a source material for the manufacturing of geopolymers. This paper presents the triaxial stress-strain characteristics of a novel geopolymer developed from basalt rock waste considering partial replacement with ground granulated blast furnace slag (GGBFS) up to 30%. A detailed mix-design investigation revealed the optimum molarity (M) of the sodium hydroxide solution to be 8M whereas the optimum ratio (R) of sodium silicate to sodium hydroxide solution as 0.75. The axial stress-strain relationships were developed after a series of triaxial laboratory tests for low confining pressures (0 to 800 kPa) and Hoek cell tests for high confining pressures (1 to 5 MPa). A constitutive model predicting the complete stress-strain behaviour has been proposed. The geopolymer stress-strain behaviour shows some degree of similarity to Portland cement binder, however, differences such as increase in stiffness and reduction in ductility were observed. The scanning electron microscopy (SEM) images also suggested a dense geopolymer gel formation resulting in a homogeneous and compact microstructure. This study demonstrates that the innovative material proposed herein produced from industrial wastes has suitable characteristics to be used as an alternative and sustainable construction material.

Keywords: basalt rock waste, ground granulated blast furnace slag (GGBFS), geopolymer, microstructure, triaxial, stress-strain behaviour

Introduction

Basalt rocks, due to their high aluminosilicate content, can be a potential raw material for the manufacturing of geopolymers. A basalt rock quarry can generate 20,000-30,000 tons per annum of rock waste, which is mostly disposed into landfill sites, thus contributing to environmental hazards (Eliche-Quesada et al., 2020). This waste can be utilised in the development of a new geopolymer which can find its usage in the construction industry and contribute towards sustainable civil engineering materials.

The geopolymer based concrete and cementitious binders have been receiving significant attention in the past decade. Geopolymers are synthesized as a result of activation of aluminosilicate source by a highly concentrated alkali hydroxide or silicate solution (Azevedo et al., 2020; Davidovits, 1989; Haider et al., 2014; Mathew and Issac, 2020; Nawaz et al., 2020; Sajjad et al., 2021; Serag Faried et al., 2020; Xie et al., 2020). The geopolymers derived from metakaolin, sedimentary rock powders, fly ash, blast furnace slag and other materials have shown similar compressive strengths (Görhan and Kürklü, 2014; Lahoti et al., 2017; Nath and Kumar, 2019; Top and Vapur, 2018), enhanced chloride and sulphate resistance characteristics (Kwasny et al., 2018; Reddy et al., 2013; Sata et al., 2012; Sturm et al., 2018; Wasim et al., 2021), cost reduction up to 30% and lower greenhouse gas emissions (Erfanimanesh and Sharbatdar, 2020; Kolovos et al., 2013; Shobeiri et al., 2021; Zhang et al., 2013) as compared to conventional cementitious binders.

However, in the previous literature, there has been little investigation related to the constitutive behaviour of different geopolymers under active confinement pressures (Haider et al., 2014). This is critical to understand the complete stress-strain response of engineering materials, which underpins their wide application in infrastructure projects. Past studies have reported stress-strain behaviours under lateral confinement mostly for concrete only (Binici, 2005; Candappa et al., 2001; Hsu and Hsu, 1994; Lokuge et al., 2005; Montoya et al., 2006; Popovics, 1973; Samani and Attard, 2012; Sargin et al., 1972; Xiao et al., 2010). The models proposed were able to predict load-deformation behaviour of concrete confined using high tensile materials. Such models can provide a better understanding of constitutive behaviour of Portland cement concrete used in several civil engineering applications such as concrete columns confined using steel, fibre reinforced polymer fabrics etc. However, some other models have been produced using triaxial compression testing to develop general stress-strain relationships under different confinements. The triaxial compression models can fairly depict general material deformation characteristics of concrete under confinement and can be used for different construction applications. For instance, Candappa et al. presented triaxial stress-strain behaviour of high strength concrete (Candappa et al., 2001) which were further used by Lokuge et al. for developing a constitutive model showing stress-strain and volumetric behaviour of high strength concrete (Lokuge et al., 2005). Binici proposed an analytical model for stress-strain behaviour of concrete under triaxial compression helpful in predicting ultimate and residual strength of the material (Binici, 2005). Similarly, Montoya et al. have also explained concrete strength, pre and post peak analysis of stress strain curves under triaxial compression (Montoya et al., 2006). Triaxial compression testing is required for applications where the structure is going to experience confinement. Examples may include all buried structures such as retaining walls, tunnels and foundations. This is done for various engineering materials such as soils, rocks, concrete or any other construction material. Similar research should be performed on alkali activated geopolymers as well to investigate their shear strength behaviour under active lateral confinement. This would be beneficial in understanding the structural behaviour of geopolymers and promote their usage as a sustainable alternative construction material in several applications such as breakwater structures, retaining walls and marine infrastructure.

This study highlights the mechanical strength characteristics and the triaxial stress-strain behaviour of a novel sustainable geopolymer based on two industrial wastes; basalt rock dust and ground granulated blast furnace slag (GGBFS). The optimum values of the synthesis parameters required in the formation of the geopolymer were checked, in order to achieve higher compressive strength and better workability characteristics. The potential of basalt rock waste to be used as a precursor material on its own for geopolymer production was also investigated by the authors (Nawaz et al., 2021). The basalt rock waste being high in silica (51.1%) and alumina (15.8%) content did promote geopolymerisation; however, as calcium oxide content was relatively low, the strength gain upon geopolymerisation was small (around 2 MPa). Therefore, an addition of a calcium rich source such as GGBFS was necessary for the enhancement of calcium aluminate silicate hydrate (C-A-S-H) gel linkage formation, therefore contributing to the increase in binding strength (Mohammadinia et al., 2018).

In the current research, the stress-strain response of the basalt rock waste and GGBFS geopolymer was analysed for different confinement levels. The geopolymer samples prepared as per the optimum mix design ratios were tested using triaxial compression equipment for low confining pressures ranging from 0 to 800 kPa and using a Hoek cell apparatus for higher confining pressures ranging from 1 to 5 MPa. A new constitutive model was also proposed which successfully predicts the stress-strain behaviour of the novel material under a wide range of confining pressures. The geopolymer samples prepared were tested using triaxial compression equipment for low confinement levels ranging from 0 to 800 kPa and using a Hoek cell apparatus for higher confinement pressures ranging from 1 to 5 MPa. A new constitutive model was proposed which successfully predicts the stress-strain behaviour of the novel material under active confining pressures. The geopolymer developed from basalt rock waste and GGBFS could find its potential application in the construction industry such as brick making, concrete, mortar and ceramic manufacturing. The material possesses high compressive and shear strengths and could be used in the construction of buried structures such as tunnels and retaining walls. Further, due to geopolymers having superior performance to concrete under sulphate and chloride attacks, the material could possibly find its usage in marine infrastructure (Nawaz et al., 2020). The proposed geopolymer could also be used as a soil stabilising agent in many in-situ ground improvement techniques such as deep soil mixing, where an auger-mixing tool is drilled down to a predesigned depth while injecting and mixing a cementitious binder with the in-situ soil (Yaghoubi et al., 2019). The soil treated through this technique would have circular columns of stabilised soil and thus the engineering properties of the in-situ soil could be improved. Such applications of the proposed geopolymer can result in substantial economic and environmental benefits and will contribute to enhanced sustainable construction practices.

Experimental program

Raw materials acquisition and characterisation

The geopolymer samples were prepared using two precursor materials; basalt rock waste and ground granulated blast furnace slag (GGBFS). The basalt rock waste was procured from a quarry in the Illawarra region of New South Wales (Australia) whereas GGBFS was provided by the Australasian Slag Association (ASA). The alkali activator solution was prepared using 98% pure sodium hydroxide pellets manufactured by Bondall (Australia) and D-grade sodium silicate solution (specific gravity= 1.53 and SiO_2/Na_2O modulus ratio=2.0) supplied by PQ Corporation (Australia).

In order to investigate the general geotechnical characteristics of basalt rock waste, several identification and characterisation tests such as particle size analysis, Atterberg limits analysis, specific gravity analysis and standard Proctor compaction tests were performed in a preliminary study by the authors (Nawaz et al., 2021). The particle size distribution curves for basalt rock waste and GGBFS are shown in Figure 1. The D_{10}, D_{30} and D_{50} for basalt fines were 3.5µm, 17.5µm and 40.5µm while the D_{10}, D_{30} and D_{50} for GGBFS were found to be 1.3µm, 2.1µm and 3.9µm. Standard Proctor compaction tests revealed the maximum dry unit weight and optimum moisture content of the basalt rock waste to be 18.8 kN/m^3 and 13.5%, respectively as shown in Figure 2. The specific gravity of basalt rock waste was found to be 2.76. The basalt fines showed a liquid limit of 24.0%, plastic limit of 17.6% and a plasticity index of 6.4%. Thus, the basalt rock waste could be classified as clayey silt or CL-ML.

Scanning electron microscopy (SEM) images were obtained to investigate the microstructure of basalt rock waste using JEOL JSM-6490LV scanning electron microscope. The images taken at different magnifications (x250, x500, x1000 and x2000) can be seen in Figure 3. The scanning electron micrographs revealed that the basalt waste particles have sharp-edged angular surfaces that assist in greater interlocking and thus denser geopolymer gel formation. A combination of different particle sizes is expected to contribute towards pore size reduction of geopolymer matrix. The voids in the sample imaged ranged from 4 to 8 µm and were likely to be reduced during the geopolymerisation process. The energy dispersive spectroscopy (EDS) analysis showed high Si and Al peaks, as highlighted in Figure 4, which was a confirmation of basalt fines being a suitable aluminosilicate source for geopolymerisation. The silicon and aluminium content present in the basalt waste would undergo dissolution and hydrolysis upon activation by an alkaline reagent MOH where M is an alkali or alkaline earth cation (usually Na^+, K^+ etc.) as per the following reactions,

$$Al_2O_3 + 3H_2O + 2OH^- \longrightarrow 2[Al(OH)_4]^- \qquad (1)$$

$$SiO_2 + 2OH^- \longrightarrow [SiO_2(OH)_2]^{2-} \quad (2)$$

The alkali aluminosilicate reaction is expected to be followed by the formation of a gel, which continues to rearrange and reorganize its amorphous 3-D structure. Thus, the new matrix developed would be having multiple gel phases. Hardening is witnessed in the final stage where the entire matrix is polymerized and becomes a solidified mass. The chemical composition was determined through X-ray fluorescence (XRF) analysis of the basalt rock waste and GGBFS and is presented in Table 1. It can be observed that the basalt rock waste is composed mainly of aluminosilicate compounds i.e. silica, SiO_2 = 51.15% and aluminium oxide, Al_2O_3 = 15.89% by mass. In contrast, the GGBFS composition showed a high percentage of calcium oxide, CaO = 42.71% which indicated that it is highly reactive and can assist in the formation of a strong geopolymeric gel.

Mix design ratios

To obtain the optimum synthesis parameters for basalt rock waste and ground granulated blast furnace slag geopolymer, different combinations of varying parameters such as molarity (M) of sodium hydroxide solution, sodium silicate to sodium hydroxide ratio (R) and ground granulated blast furnace slag content were taken into consideration while preparing the test matrix as shown in Table 2. The sodium hydroxide (NaOH) solutions were prepared at different molar concentrations (M) such as 4M, 8M and 12M to investigate the effect of concentration of alkali activator. While several past studies reported using sodium hydroxide solutions having molarities ranging from 2M to 14M for fly-ash and slag based geopolymers (Görhan and Kürklü, 2014; Jafari Nadoushan and Ramezanianpour, 2016; Lahoti et al., 2017; Laskar and Talukdar, 2017; Lee et al., 2019; Nath and Kumar, 2019; Reddy et al., 2013; Williamson and Juenger, 2016), in this study 4, 8 and 12M were selected because they cover a wide range of molar concentrations for which maximum efficiency in geopolymerization process and larger strength gains are achieved. However, the authors acknowledge that working with high molarities may pose some risks such as skin burns and inhalation of toxic vapours. Therefore, a careful risk assessment and safe operation procedures are required both in laboratory and commercial practice. Utmost care should be exercised as per the directions in the material safety data sheet for sodium hydroxide, during handling, preparation and storage of concentrated solutions. Chemical resistant nitrile gloves should be worn to avoid skin contact. Respiratory masks should be used to avoid inhalation of vapours during mixing of NaOH pellets in water. Safety glasses should also be worn to avoid any eye damage in case of spillage. All such safety measures were adopted by the authors while carrying out the experiments. The sodium hydroxide solution was kept at ambient conditions for 24 hours to achieve equilibrium. This is consistent with past studies (Lahoti et al., 2018; Mehta and Siddique, 2017).

Specimens having different sodium silicate (Na_2SiO_3) to sodium hydroxide solutions weighted ratios (R) such as 0.25, 0.5 and 0.75 were prepared. The alkali activator solution to basalt waste dust ratio was kept constant at 0.135. This value was selected because it corresponds to the optimum moisture content for basalt rock waste, whereas the quantity of binder solids was maintained as per the maximum dry unit weight.

The basalt rock waste being the main precursor material was partially replaced with GGBFS at 10, 20 and 30% by mass. These percentages were selected in order to supplement the calcium content of the geopolymer for enhanced gel-linkages which contributed towards high compressive strength. The texture of the binder gel is improved by calcium which further increases the pH of the system and promotes rapid hydration process (Arulrajah et al., 2017). Any higher percentages would increase the strength gain process but reduce the setting time of the mix, thus compromising on the workability of the geopolymer. Further, these percentages are also in line with the previous studies, where different geopolymers were produced by partial replacement of constituting materials (Bai et al., 2019; Yang et al., 2017).

Preparation of specimens

The sodium silicate and sodium hydroxide solutions were mixed in a glass beaker at specific ratios (R), i.e. 0.25, 0.5 and 0.75 for about 30 to 40 minutes. The solution prepared was then added to the basalt rock waste at the ratios mentioned in Table 2 and mixed for 5 to 7 minutes to ensure homogeneous mixing. Cylindrical specimens, 38 mm in diameter and 76 mm in height were prepared in steel moulds and compacted statically in 3 layers using a compression frame to achieve a maximum dry unit weight of 18.8kN/m^3. Triplicate specimens were prepared for each specific ratio to ensure repeatability of results and average values for the compressive strengths were reported.

Once compacted, the specimens prepared were then wrapped in polyethylene films, sealed in polyethylene resealable bags, and cured at ambient conditions for 7 days under relatively constant temperature (approximately 22°C) and humidity (approximately 95%).

Unconfined compressive strength tests

The unconfined compressive strength (UCS) tests were carried out in accordance with AS 5101.4-2008 using 500 kN Instron universal testing machine adopting a strain rate of 0.5 mm/min. The measurement accuracy of the load cell and deformation transducers used was 0.01 N and 0.01 µm, respectively.

Triaxial compressive strength and Hoek cell tests

The triaxial compressive strength tests were carried out using Wykeham Farrance Tritech 100 kN triaxial compression machine. The compression frame assembly with a load cell capacity of 100 kN was used with the test set up to apply deviator stress to the specimen at a strain rate of 0.5 mm/min. The linear variable differential transducer (LVDT) was attached to the cell assembly to measure axial deformation. The measurement accuracy of the load cell and deformation transducers used was 0.001 N and 0.01 μm, respectively. The confining pressure system to the triaxial cell was applied using a bladder assembly driven by air pressure. The geopolymer specimens were tested at 200, 400, 600 and 800 kPa confinement pressures.

For higher confinement range, the geopolymer samples were tested using a Hoek cell apparatus. Cylindrical specimens having diameter as 45 mm and height as 90 mm were prepared for the testing. Strain gauges were attached to the specimens in order to measure lateral deformation during shearing. The specimens were then encased in the rubber sealing sleeve very carefully, to avoid any damage to the connections of the strain gauges. The sleeve was then inserted into the main steel cell body whereas top and bottom spherical seats were placed to grab the sample into position. Once the cell was placed in the compression testing machine, the pipe connecting the hydraulic oil assembly was fixed with the steel cell body in order to generate the desired confining pressures using the lever arm. Once the confining pressure was achieved, it was locked using a valve attached to the oil cylinder. The specimens were tested at 1, 2, 3, 4 and 5 MPa confining pressures in order to assess the shear strength performance of basalt waste and GGBFS based geopolymer under high confinement. The lower confining pressure range (0 to 800 kPa) was not sufficient to adequately characterise the stress-strain response of the material. In addition, for applications such as tunnels and retaining walls, where larger lateral stresses may be present, it is important to investigate the material behaviour at higher confinement levels. Therefore, the material had to be tested under a wide range of confining pressures that could assist in developing the stress-strain model for this novel material.

Results and discussion

Effect of molar concentration of alkali activator solution

The concentration of alkaline activator solution plays a vital role in the reactivity, pore microstructure, aluminosilicate gel matrix formation as well as other mechanical properties of geopolymers (Ma et al., 2012; Rashad and Zeedan, 2011; Ruiz-Santaquiteria et al., 2012). It can be observed that that the geopolymer mix exhibited higher unconfined compressive strength values for 8M concentrations (i.e. up to 21 MPa for 30% replacement with blast furnace slag). This is likely associated with the fact that higher molarity favours better reactivity with the aluminosilicate source but only up to an optimum value of 8M. This indicates that the aluminosilicate content would experience a higher extent of dissolution to complete the process of geopolymerisation. Once an optimum value is exceeded, the precipitation of dissolved species inhibits geopolymerisation. A summary of the average unconfined compressive strength results is given in Figure 5.

The molarities higher than the optimum value can hinder the complete geopolymeric gel formation (Görhan and Kürklü, 2014; Jafari Nadoushan and Ramezanianpour, 2016; Williamson and Juenger, 2016). These findings are consistent with the results reported in past studies for other geopolymer sources, in which a decrease in compressive strengths beyond optimum value of alkaline concentration was attributed to increased viscosity of activator solution and the presence of unreacted silica and alumina (Barbosa et al., 2000; Hardjito et al., 2008; Jafari Nadoushan and Ramezanianpour, 2016; Williamson and Juenger, 2016). As the material became stiffer at 8M concentrations, it tend to be more brittle whereas the incomplete reactions, free silica in the system and increased viscosity of activator solution at 12M concentration samples resulted in a weak geopolymeric gel, thus contributing to a decrease in compressive strength as well as a more ductile behaviour (Barbosa et al., 2000; Hardjito et al., 2008; Nawaz et al., 2021; Williamson and Juenger, 2016). Furthermore, 12M samples were found to set quicker probably due to accelerated geopolymerisation reactions, which hindered the compaction process and workability.

Based on the results reported herein, the optimal molarity of sodium hydroxide solution for the basalt rock waste and ground granulated blast furnace slag geopolymer was found to be 8.0 M.

Effect of sodium silicate to sodium hydroxide ratio

From the initial mixes, it was found that the unconfined compressive strength (UCS) values increased with the increase in the sodium silicate to sodium hydroxide ratios (R) from 0.25 to 0.75R. As illustrated in Figure 5, the peak axial stress value for 8M-0.25R-30% BFS specimens was 21 MPa, increased to 32 MPa for 0.5R and further increased to 34 MPa for 0.75R ratios. The peak axial stress value for 12M-0.25R-10% BFS samples was about 7 MPa, increased to 8.2 MPa for 0.5R and further increased to 9.4 MPa for 0.75R ratios. The peak axial stress value for 12M-0.25R-20% BFS samples was 12.5 MPa, increased to 15.1 MPa for 0.5R and further reached 19.4 MPa against 0.75R. The peak axial stress value for 12M-0.25R-30% BFS samples was 17.5 MPa, increased to 18.7 MPa for 0.5R and further reached 20.4 MPa against 0.75R.

This trend is consistent with the results reported for geopolymers developed from other established raw materials where the increase in R values have contributed to increase in compressive strengths (Paija et al., 2020). However, it was also observed that with the increase in R values, the workability for compaction of samples decreased. The samples with the R value 0.25 were relatively easier to compact. As the values increased to 0.5 and then 0.75, the rate of geopolymerisation was accelerated due to higher content of sodium silicate solution causing earlier setting of the mix, thus making it difficult to compact.

Based on the results reported herein, the optimal ratio of sodium silicate to sodium hydroxide solution (R) for the basalt rock waste and ground granulated blast furnace slag geopolymer was found to be 0.75.

Effect of ground granulated blast furnace slag (GGBFS)

The strength gain in many geopolymer materials is sometimes slow due to lack of calcium content in various precursors, which may result in a higher setting time (Cho et al., 2017). Under such circumstances, addition of high calcium additives such as ground granulated blast furnace slag may assist in accelerating the chemical reactions and facilitate the attainment of high early strength (Chindaprasirt et al., 2011; Deb et al., 2014; Sajjad et al., 2022). The mass of basalt waste in the geopolymer precursor mix was partially replaced by 10, 20 and 30% to analyse the compressive strength behaviour.

Figure 5 shows that the peak axial stresses increase with larger content of GGBFS i.e. 11 MPa, 28 MPa and 34 MPa for 10, 20% and 30% replacement, respectively. This is likely associated with the accelerated geopolymerisation reactions which are facilitated by calcium content in the system derived from higher percentage of GGBFS. This in turn led to the formation of a denser, monolithic and a less porous microstructure geopolymer which achieved high early compressive strengths. The 7-day unconfined compressive strength is considered as a benchmark for geopolymers, as more than 75% of the geopolymerisation mechanism takes place within the first 7 days. The 7-day strengths of geopolymers manufactured from metakaolin, fly-ash and slag for bricks, mortar and concrete applications usually lie in the range from 25 to 40 MPa (Ahmad et al., 2021; Ali et al., 2020). The specimens reported here using partial replacement of basalt waste with GGBFS at 10%, 20% and 30% conform to the similar strength values and can be used for different applications such as geopolymer bricks and concrete manufacturing.

Considering the strength, workability and microstructure characteristics reported in previous sections, the optimum GGBFS replacement percentage required to achieve comparable performance to more established geopolymers is 30%. However, it should be noted that smaller replacement percentages may be considered for applications where compressive strengths exceeding 30 MPa are not required.

Microstructure analysis

Figure 6 shows the SEM micrographs of basalt rock waste and 30% blast furnace slag geopolymer (8M-0.75R-30%BFS in particular) at 7 days and 28 days, respectively. It can be observed that a well compacted and dense gel formation occurs in the first seven days of geopolymerisation when the material has experienced most of the chemical reactions and entered its hardening stage. The gel formed is monolithic in nature and pore size is estimated to be reduced to around 3μm as compared to the 8μm exhibited in the original basalt fines microstructure There is not much significant difference in 28 days images as after the first week, the rate of geopolymerisation is slow.

Triaxial compression and Hoek cell tests

To investigate the stress-strain behaviour further, a series of triaxial compression tests were conducted on specimens prepared with the optimum mix, i.e. 8M-0.75R-30%BFS. To ensure full saturation conditions were achieved, the specimens prepared were kept submerged in water for a period of about 6 months under relatively constant temperature environment. This condition mimics that of materials that are used in marine environments and assisted in the evaluation of its suitability for these conditions. After a 6 months submersion, the saturation level was checked by evaluating the magnitude of the B value. The B value was found to be 0.29. While this value may be considered rather small for particulate materials, similar values have been reported for soft rocks tested in fully saturated states (P. V. Lade, 1973).

The specimens were tested under 200, 400, 600 and 800 kPa confinement pressures. However, due to limitation of the equipment, the specimens were tested using Hoek cell apparatus for higher confinement levels of 1, 2, 3, 4 and 5 MPa. The stress strain curves produced can be seen in Figure 7. The peak axial stress values increased with increasing confining levels. For instance, the peak axial stress was 44.6 MPa against a confining pressure of 200 kPa, increase to 46.03 for 400 kPa, 47.5 for 600 kPa, 48.6 against 800 kPa, 49.9 for 1 MPa, 55.1 for 2 MPa, 59.86 for 3 MPa, 64.2 for 4 MPa and 68.3 MPa against 5 MPa confining pressures. The secant modulus (E_{50}) and peak strain energy (E_u) of the geopolymer specimens tested under different confining pressures were determined from stress strain curves shown in Figure 7. E_{50} is defined as the elastic stiffness of the material and is taken as the slope of a straight line from the origin to the 50% of peak stress value whereas E_u is the energy absorption capacity or peak strain energy and is adopted as a measure of toughness of the material. It is determined by calculating the area under the stress-strain curve up to the peak stress (Salimi and Ghorbani, 2020). The secant modulus (E_{50}) of the optimum mix design specimen ranged from 9.53 to 9.64 GPa and showed slight increase under different confining pressures as shown in Figure 8 (a). The peak strain energy (E_u) values were found to be in the range of 163 to 213 kJ/m^3 as the confining pressures were increased from 0.2 to 0.8 MPa. However, in case of the higher confining pressures from 1 to 5 MPa, a significant increase was witnessed and the values of E_u now ranged from 229 kJ/m^3 to 689 kJ/m^3 as shown in Figure 8 (b). The trend showed that more energy was required to deform the specimens as they were subjected to higher confining levels. At higher confinement levels the material became stiffer and increase in peak axial strains was observed. The pore water pressure measurement system was only available for specimens that were tested under lower confinement levels. Their values also increased with the increase in confinement as seen in Figure 9.

Model parameters development

The inherent deformation behavior of any material is described by different parameters associated to several stress-strain model equations. Due to not much work being reported in the past literature about modelling of Portland cement paste, this study considers Portland cement concrete, a conventional construction material, as a basis of comparison and obtaining different model parameters for basalt rock waste and ground granulated blast furnace slag geopolymer.

Peak confined axial stress

One of the fundamental parameters needed to model the constitutive relationship of a material under lateral confinement is the peak axial stress. There are different equations available to predict the peak stress of confined concrete (Ahmad et al., 2021). The general form of equation mostly followed is shown in Eq. (3) which is the relationship at a multi-axial state of stress and can be demonstrated reasonably as follows.

$$\frac{\sigma_1}{f_{co}} = 1 + k_1 \frac{\sigma_3}{f_{co}} \tag{3}$$

Where σ_1 and σ_3 are the peak stress of confined specimen and lateral confinement pressure, respectively. The unconfined peak compressive stress is denoted by f_{co} and k_1 is a curve fitting factor. Many researchers have proposed different values of k_1 for their individual studies. However, as the geopolymer material tested in this study is novel, the k_1 value for this study was determined using regression analysis as shown in Figure. 10. It was found that a linear relationship was quite accurate at higher confinement levels, however, at lower confinement pressures it was not suitable. Therefore, a novel parabolic relationship was adopted for modelling the peak axial stress at various confinement levels and is shown in Eq. (4) as follows,

$$\frac{\sigma_1}{f_{co}} = 1 + k_1 (\frac{\sigma_3}{f_{co}})^m \tag{4}$$

Based on the regression analysis, a k_1 factor of 2.89 and m value of 0.68 is proposed for the triaxial stress state of the basalt waste geopolymer. The k_1 value is comparable to the reported value of 3.2 to 3.5 in literature and thus shows that the increase in strength of the geopolymer under lateral confinement pressures is similar in trend to the Ordinary Portland cement concrete.

Peak confined axial strain

For obtaining the relationship between axial strain at peak axial stress under active lateral confinement, the experimental data was fitted using a linear regression analysis as shown in Figure. 11. The general form of equation for the confined concrete under triaxial stress state is shown in Eq. (5)

$$\frac{\varepsilon_{cc}}{\varepsilon_{co}} = 1 + k_2 \frac{\sigma_3}{f_{co}} \quad (5)$$

Where ε_{cc} and ε_{co} are the strains at peak stress of confined and unconfined specimens, respectively. Linear regression analysis was carried out to determine the value of k_2 and is illustrated in Figure 11.

The Eq. (5) can be re-written with the best-fit parameter of 12.04 as follows,

$$\frac{\varepsilon_{cc}}{\varepsilon_{co}} = 1 + 12.04 \frac{\sigma_3}{f_{co}} \quad (6)$$

It was found that higher values of material constant k_2 in Eq. (6) could mean higher failure strains due to lateral confinement. This value of 12.04 found for basalt rock waste geopolymer is much lower than reported value of 17 to 18 in literature for Ordinary Portland cement concrete. This shows that basalt rock waste geopolymer exhibits less deformation in axial direction than conventional concrete under lateral confinement.

Stress-strain equation

Several approaches have been made in modelling the stress-strain behavior of concrete and its composite materials (Hsu and Hsu, 1994; Popovics, 1973; Samani and Attard, 2012). In this study, a linear behavior was observed in the ascending branch until elastic limit and a non-linear trend was seen post peak stress. The stress-strain model proposed by Mander et al. (Mander et al., 1988) for confined concrete was adopted for basalt geopolymer under triaxial stress state with some modifications and is presented in Eqs. (7) and (8).

$$\frac{f_c}{\sigma_1} = \frac{xr}{r - 1 + x^r} \quad (7)$$

$$x = \frac{\varepsilon_c}{\varepsilon_{cc}} \quad (8)$$

where f_c and ε_c are the stress and strain, respectively, at any point on the stress-strain curve; σ_1 and ε_{cc} are the peak stress of confined specimen and corresponding strain, respectively; r is the curve fitting factor. The factor *r* was calculated using Eq. (9), as suggested by Mander et al. (Mander et al., 1988)

$$r = \frac{E_c}{E_c - E_{sec}} \quad (9)$$

Where E_c and E_{sec} are the modulus of elasticity and secant modulus of elasticity of basalt geopolymer, respectively. The value of E_c (MPa) can be determined using Eq. (10), respectively, as suggested by Sarker (Nath and Sarker, 2017) by using modified Australian standard AS 3600-2009.

$$E_c = \alpha\ x\ (\rho)^{1.5} x\ (\beta\sqrt{f_{cmi}}) \quad (10)$$

Where ρ is the density of the material in kg/m^3, α is a modifying factor proposed as 0.75, β is the conversion factor used as 0.043 and f_{cmi} is the mean in-situ compressive strength taken as 90% of unconfined compressive strength f_{co} of the basalt geopolymer. Mander et al. suggested to calculate the E_{sec} using Eq. (11).

$$E_{sec} = \frac{\sigma_1}{\varepsilon_{cc}} \quad (11)$$

The comparison between the analytical model presented in Figure 12 and the experimental results revealed that the stress-strain model proposed in this study provided a good correlation with the experimental stress-strain curves of the basalt rock waste geopolymer specimens.

Volumetric dilation and contraction

To evaluate the volumetric changes in the basalt rock waste geopolymer under the high lateral confinement pressures, normalized volumetric strain factor (ε_{vnorm}) was plotted against normalized axial strain factor (ε_{anorm}) as shown in Figure 13. The factors are described in Eq. (12) and Eq. (13) respectively.

$$\varepsilon_{vnorm} = \frac{\varepsilon_v}{\varepsilon_{vmax}} \quad (12)$$

$$\varepsilon_{anorm} = \frac{\varepsilon_a}{\varepsilon_{amax}} \quad (13)$$

The normalized volumetric strain factor (ε_{vnorm}) is obtained as the ratio of volumetric strain (ε_v) to the maximum value of volumetric strain (ε_{vmax}) whereas the normalized axial strain factor (ε_{anorm}) is calculated as the ratio of axial strain to the axial strain at peak axial stress. The volumetric strain exhibited an increasing trend. It reached a maximum value after which it started to decrease as shown in Figure 13. The descending branch then touched the zero line beyond which the values dropped in the negative region. This behaviour confirmed that the geopolymer sample initially contracted under the lateral confinement, then reached to a maximum contraction level, after which it witnessed expansion. At a specific level of axial strain, the sample returned somewhat to its original volume. This behaviour was found to be independent of the level of confining pressure.

Nash-Sutcliffe Efficiency Index (E_f)

To evaluate the goodness of fit of any linear model, the use of correlation coefficient and standard error of estimate has been common. However, due to some limitations of correlation coefficient for power models, Nash and Sutcliffe (McCuen et al., 2006) proposed a factor called efficiency index (E_f) as an alternative to measure the fitting quality of such models as shown in Eq. (14). The efficiency index was calculated for peak axial stress prediction using the stress-strain model proposed in this study for the novel geopolymer material.

$$E_f = 1 - [\frac{\Sigma(Y_i^* - Y_i)^2}{\Sigma\left(Y_i - Y_{avg}\right)^2}] \tag{14}$$

Where E_f is the Nash-Sutcliffe efficiency index, Y^*_i is the predicted value, Y_i is the measured value and Y_{avg} is the average of the measured value of the variable. It was found that E_f values against both low and high confinement pressures were found to be ranging between 0.97 and 0.99 as shown in Table 3, depicting high precision for the model proposed for this material.

Economic and environmental benefits

The cost of any material is one of the major deciding factors for its application in the construction industry. The use of industrial wastes in the manufacturing of civil engineering materials can prove to be beneficial in terms of cost reduction as well as lowering the carbon footprint of construction activities (Mohammadinia et al., 2018). A cost comparison study was conducted and quotations from different supplier companies such as PQ Corporation Australia, Bondall Australia, Boral Australia and Australasian Slag Association were obtained. The average cost of some conventional precursor materials used in the synthesis of geopolymers are for instance, fly-ash costs about AU$ 600/tonne, metakaolin around AU$ 550/tonne and

GGBFS around AU$ 80/tonne. The alkaline activator sodium hydroxide solution costs around AU$ 9000/tonne whereas sodium silicate solution may cost around AU$ 6500/tonne. Using basalt dust waste and GGBFS geopolymer in the mix proportions suggested above, the per cubic meter cost can range from AU$ 1000 to AU$ 1200 thus reducing the cost by up to 50% as compared to conventional fly-ash based geopolymers. The study presented here is an example with the assumption that the raw materials are readily available in the vicinity of where the geopolymer is being produced. However, in more remote locations where quarried fines waste may not be available, the cost of transport may incline the decision towards the use of more established precursors materials. Hence, a thorough economic feasibility study should be performed on a project to project basis.

The use of basalt rock waste and GGBFS geopolymer may result not only in a reduced burden on stockpiling in landfills but also towards lower greenhouse gas (GHG) emissions as compared to already established construction materials such as Ordinary Portland Cement (OPC) and geopolymers manufactured from fly-ash, metakaolin etc. A carbon footprint comparison study was performed for different civil engineering materials exhibiting comparable compressive strengths. It was found that the optimum mix design of the basalt rock waste and GGBFS geopolymer had the lowest GHG emissions, summing up to 67.6 kg $CO_{2\ eq.}$ per ton production of the material whereas the OPC exhibited the highest emissions at about 963 kg $CO_{2\ eq.}$ per ton. A comparison chart can be seen below in the Figure 14.

Conclusions

This study highlights the triaxial stress-strain characteristics of a novel geopolymer developed using basalt rock waste and ground granulated blast furnace slag. The specimens obtained from the optimum mix design of the geopolymer based on compressive strength and workability were tested under low confining pressures (0 to 800 kPa) through a series of triaxial compression tests and high confining pressures (1 to 5 MPa) using a Hoek cell. A constitutive relationship was also proposed to predict the stress-strain behaviour of this new material under lateral confinement. The main conclusions that can be drawn from this study can be summarised as follows:

1. The optimum molarity of sodium hydroxide activator solution (M) was 8M while the optimum weighted ratio of the sodium silicate to sodium hydroxide solution (R) was found to be 0.75. The slag content of 30% was found to be optimum, to achieve a 7-day unconfined compressive strength of 34 MPa. The SEM micrographs revealed that the microstructure developed in the first week was highly monolithic and dense, with a reduced pore size, therefore contributing to high early strengths.

2. The constitutive model presented successfully predicts the stress-strain behaviour of the geopolymer under a range of confining pressures. The k_1 factor for the relationship between peak axial stress at varying confinement levels was found to be 2.89. The value is comparable to the reported value of 3.2 to 3.5 for Ordinary Portland cement concrete in past studies and shows a similar trend for the increase in strength of the material.

3. The k_2 factor for the relationship of axial strain at peak axial stress with confinement ratio is 12.04 for this geopolymer which is much lower than reported value of 17 for Ordinary Portland cement concrete. It shows that the geopolymer developed exhibits less deformation in axial direction than conventional concrete under lateral confinement. The material undergoes contraction under active lateral confinement and then starts to dilate after a certain point rapidly indicating the reduced ductility of geopolymer as compared to Ordinary Portland cement concrete.

Data Availability Statement

All data, models and code generated or used during the study appear in the published article.

Acknowledgements

The authors gratefully acknowledge the financial assistance for the first author from Higher Education Commission (Pakistan) through the Human Resource Development Initiative - Faculty Development Program. Laboratory assistance by Mr. Richard Berndt, Mr. Duncan Best and Mr. Travis Marshall is highly appreciated. The supply of materials from local quarries, PQ Australia and Australasian Slag Association (ASA) is also recognised.

CRediT Author statement

The paper is a joint contribution of all authors but specific contributions can be recognised as follows,

Mohsin Nawaz: Methodology, Writing - Original Draft, Laboratory experiments

Ana Heitor: Conceptualization, Writing - Review & Editing, Resources, Supervision, Project administration

Muttucumaru Sivakumar: Conceptualization, Writing - Review & Editing, Resources, Supervision

Declaration of Interest Statement

The authors declare that they have no known competing financial interests or personal relationships that could have appeared to influence the work reported in this paper.

5. References

Ahmad, J., Yu, T., Hadi, M.N.S., 2021. Basalt Fiber-Reinforced Polymer-Confined Geopolymer Concrete. ACI Structural Journal 118(1), 289-300.

Ali, S., Sheikh, M.N., Sargeant, M., Hadi, M.N.S., 2020. Influence of Polypropylene and Glass Fibers on Alkali- Activated Slag/Fly Ash Concrete. ACI Structural Journal 117(4).

Arulrajah, A., Mohammadinia, A., D'Amico, A., Horpibulsuk, S., 2017. Effect of lime kiln dust as an alternative binder in the stabilization of construction and demolition materials. Construction and Building Materials 152, 999-1007.

Azevedo, A.R.G., Vieira, C.M.F., Ferreira, W.M., Faria, K.C.P., Pedroti, L.G., Mendes, B.C., 2020. Potential use of ceramic waste as precursor in the geopolymerization reaction for the production of ceramic roof tiles. Journal of Building Engineering 29, 101156.

Bai, T., Song, Z., Wang, H., Wu, Y., Huang, W., 2019. Performance evaluation of metakaolin geopolymer modified by different solid wastes. Journal of Cleaner Production 226, 114-121.

Barbosa, V.F.F., MacKenzie, K.J.D., Thaumaturgo, C., 2000. Synthesis and characterisation of materials based on inorganic polymers of alumina and silica: Sodium polysialate polymers. International Journal of Inorganic Materials 2(4), 309-317.

Binici, B., 2005. An analytical model for stress–strain behavior of confined concrete. Engineering Structures 27(7), 1040-1051.

Candappa, D.C., Sanjayan, J.G., Setunge, S., 2001. Complete Triaxial Stress-Strain Curves of High-Strength Concrete. Journal of Materials in Civil Engineering 13(3), 209-215.

Chindaprasirt, P., Chareerat, T., Hatanaka, S., Cao, T., 2011. High-Strength Geopolymer Using Fine High-Calcium Fly Ash. Journal of Materials in Civil Engineering 23(3), 264-270.

Cho, Y.-K., Yoo, S.-W., Jung, S.-H., Lee, K.-M., Kwon, S.-J., 2017. Effect of Na2O content, SiO2/Na2O molar ratio, and curing conditions on the compressive strength of FA-based geopolymer. Construction and Building Materials 145, 253-260.

Davidovits, J., 1989. Geopolymers and geopolymeric materials. Journal of thermal analysis 35(2), 429-441.

Deb, P.S., Nath, P., Sarker, P.K., 2014. The effects of ground granulated blast-furnace slag blending with fly ash and activator content on the workability and strength properties of geopolymer concrete cured at ambient temperature. Materials & Design (1980-2015) 62, 32-39.

Eliche-Quesada, D., Ruiz-Molina, S., Pérez-Villarejo, L., Castro, E., Sánchez-Soto, P.J., 2020. Dust filter of secondary aluminium industry as raw material of geopolymer foams. Journal of Building Engineering 32, 101656.

Erfanimanesh, A., Sharbatdar, M.K., 2020. Mechanical and microstructural characteristics of geopolymer paste, mortar, and concrete containing local zeolite and slag activated by sodium carbonate. Journal of Building Engineering 32, 101781.

Görhan, G., Kürklü, G., 2014. The influence of the NaOH solution on the properties of the fly ash-based geopolymer mortar cured at different temperatures. Composites Part B: Engineering 58, 371-377.

Haider, G.M., Sanjayan, J.G., Ranjith, P.G., 2014. Complete triaxial stress–strain curves for geopolymer. Construction and Building Materials 69, 196-202.

Hardjito, D., Cheak, C.C., Ing, C.H.L., 2008. Strength and setting times of low calcium fly ash-based geopolymer mortar. Modern Applied Science 2(4), 3-11.

Hsu, L.S., Hsu, C.-T.T., 1994. Complete stress — strain behaviour of high-strength concrete under compression. Magazine of Concrete Research 46(169), 301-312.

Jafari Nadoushan, M., Ramezanianpour, A.A., 2016. The effect of type and concentration of activators on flowability and compressive strength of natural pozzolan and slag-based geopolymers. Construction and Building Materials 111, 337-347.

Kolovos, K.G., Asteris, P.G., Cotsovos, D.M., Badogiannis, E., Tsivilis, S., 2013. Mechanical properties of soilcrete mixtures modified with metakaolin. Construction and Building Materials 47, 1026-1036.

Kwasny, J., Aiken, T.A., Soutsos, M.N., McIntosh, J.A., Cleland, D.J., 2018. Sulfate and acid resistance of lithomarge-based geopolymer mortars. Construction and Building Materials 166, 537-553.

Lahoti, M., Wong, K.K., Tan, K.H., Yang, E.-H., 2017. Use of alkali-silica reactive sedimentary rock powder as a resource to produce high strength geopolymer binder. Construction and Building Materials 155(Supplement C), 381-388.

Lahoti, M., Wong, K.K., Yang, E.-H., Tan, K.H., 2018. Effects of Si/Al molar ratio on strength endurance and volume stability of metakaolin geopolymers subject to elevated temperature. Ceramics International 44(5), 5726-5734.

Laskar, S.M., Talukdar, S., 2017. Preparation and tests for workability, compressive and bond strength of ultra-fine slag based geopolymer as concrete repairing agent. Construction and Building Materials 154, 176-190.

Lee, W.-H., Wang, J.-H., Ding, Y.-C., Cheng, T.-W., 2019. A study on the characteristics and microstructures of GGBS/FA based geopolymer paste and concrete. Construction and Building Materials 211, 807-813.

Lokuge, W.P., Sanjayan, J.G., Setunge, S., 2005. Stress–Strain Model for Laterally Confined Concrete. Journal of Materials in Civil Engineering 17(6), 607-616.

Ma, Y., Hu, J., Ye, G., 2012. The effect of activating solution on the mechanical strength, reaction rate, mineralogy, and microstructure of alkali-activated fly ash. Journal of Materials Science 47(11), 4568-4578.

Mander, J.B., Priestley, M.J.N., Park, R., 1988. Theoretical Stress‐Strain Model for Confined Concrete. Journal of Structural Engineering 114(8), 1804-1826.

Mathew, G., Issac, B.M., 2020. Effect of molarity of sodium hydroxide on the aluminosilicate content in laterite aggregate of laterised geopolymer concrete. Journal of Building Engineering 32, 101486.

McCuen, R.H., Knight, Z., Cutter, A.G., 2006. Evaluation of the Nash & Sutcliffe Efficiency Index. Journal of Hydrologic Engineering 11(6), 597-602.

Mehta, A., Siddique, R., 2017. Strength, permeability and micro-structural characteristics of low-calcium fly ash based geopolymers. Construction and Building Materials 141, 325-334.

Mohammadinia, A., Arulrajah, A., D'Amico, A., Horpibulsuk, S., 2018. Alkali-activation of fly ash and cement kiln dust mixtures for stabilization of demolition aggregates. Construction and Building Materials 186, 71-78.

Montoya, E., Vecchio, F.J., Sheikh, S.A., 2006. Compression Field Modeling of Confined Concrete: Constitutive Models. Journal of Materials in Civil Engineering 18(4), 510-517.

Nath, P., Sarker, P.K., 2017. Flexural strength and elastic modulus of ambient-cured blended low-calcium fly ash geopolymer concrete. Construction and Building Materials 130, 22-31.

Nath, S.K., Kumar, S., 2019. Role of alkali concentration on reaction kinetics of fly ash geopolymerization. Journal of Non-Crystalline Solids 505, 241-251.

Nawaz, M., Heitor, A., Sivakumar, M., 2020. Geopolymers in construction - recent developments. Construction and Building Materials 260, 120472.

Nawaz, M., Heitor, A., Sivakumar, M., 2021. Development and evaluation of a novel geopolymer based on basalt rock waste and ground granulated blast furnace slag. Australian Journal of Civil Engineering, 1-20.

Paija, N., Kolay, P.K., Mohanty, M., Kumar, S., 2020. Ground Bottom Ash Application for Conventional Mortar and Geopolymer Paste. Journal of Hazardous, Toxic, and Radioactive Waste 24(1), 04019025.

Popovics, S., 1973. A numerical approach to the complete stress-strain curve of concrete. Cement and Concrete Research 3(5), 583-599.

Rashad, A.M., Zeedan, S.R., 2011. The effect of activator concentration on the residual strength of alkali-activated fly ash pastes subjected to thermal load. Construction and Building Materials 25(7), 3098-3107.

Reddy, D.V., Edouard, J.-B., Sobhan, K., 2013. Durability of Fly Ash–Based Geopolymer Structural Concrete in the Marine Environment. Journal of Materials in Civil Engineering 25(6), 781-787.

Ruiz-Santaquiteria, C., Skibsted, J., Fernández-Jiménez, A., Palomo, A., 2012. Alkaline solution/binder ratio as a determining factor in the alkaline activation of aluminosilicates. Cement and Concrete Research 42(9), 1242-1251.

Sajjad, U., Sheikh, M.N., Hadi, M.N.S., 2021. Experimental study of the effect of graphene on properties of ambient-cured slag and fly ash-based geopolymer paste and mortar. Construction and Building Materials 313, 125403.

Sajjad, U., Sheikh, M.N., Hadi, M.N.S., 2022. Incorporation of graphene in slag-fly ash-based alkali-activated concrete. Construction and Building Materials 322, 126417.

Salimi, M., Ghorbani, A., 2020. Mechanical and compressibility characteristics of a soft clay stabilized by slag-based mixtures and geopolymers. Applied Clay Science 184, 105390.

Samani, A.K., Attard, M.M., 2012. A stress–strain model for uniaxial and confined concrete under compression. Engineering Structures 41, 335-349.

Sargin, M., Ghosh, S.K., Handa, V.K., 1972. Discussion: Effects of lateral reinforcement upon the strength and deformation properties of concrete. Magazine of Concrete Research 24(80), 173-174.

Sata, V., Sathonsaowaphak, A., Chindaprasirt, P., 2012. Resistance of lignite bottom ash geopolymer mortar to sulfate and sulfuric acid attack. Cement and Concrete Composites 34(5), 700-708.

Serag Faried, A., Sofi, W.H., Taha, A.-Z., El-Yamani, M.A., Tawfik, T.A., 2020. Mix Design Proposed for Geopolymer Concrete Mixtures Based on Ground Granulated Blast furnace slag. Australian Journal of Civil Engineering 18(2), 205-218.

Shobeiri, V., Bennett, B., Xie, T., Visintin, P., 2021. A comprehensive assessment of the global warming potential of geopolymer concrete. Journal of Cleaner Production 297, 126669.

Sturm, P., Gluth, G.J.G., Jäger, C., Brouwers, H.J.H., Kühne, H.C., 2018. Sulfuric acid resistance of one-part alkali-activated mortars. Cement and Concrete Research 109, 54-63.

Top, S., Vapur, H., 2018. Effect of basaltic pumice aggregate addition on the material properties of fly ash based lightweight geopolymer concrete. Journal of Molecular Structure 1163, 10-17.

Wasim, M., Ngo, T.D., Law, D., 2021. A state-of-the-art review on the durability of geopolymer concrete for sustainable structures and infrastructure. Construction and Building Materials 291, 123381.

Williamson, T., Juenger, M.C.G., 2016. The role of activating solution concentration on alkali–silica reaction in alkali-activated fly ash concrete. Cement and Concrete Research 83, 124-130.

Xiao, Q.G., Teng, J.G., Yu, T., 2010. Behavior and Modeling of Confined High-Strength Concrete. Journal of Composites for Construction 14(3), 249-259.

Xie, T., Visintin, P., Zhao, X., Gravina, R., 2020. Mix design and mechanical properties of geopolymer and alkali activated concrete: Review of the state-of-the-art and the development of a new unified approach. Construction and Building Materials 256, 119380.

Yaghoubi, M., Arulrajah, A., Disfani, M.M., Horpibulsuk, S., Darmawan, S., Wang, J., 2019. Impact of field conditions on the strength development of a geopolymer stabilized marine clay. Applied Clay Science 167, 33-42.

Yang, T., Zhu, H., Zhang, Z., 2017. Influence of fly ash on the pore structure and shrinkage characteristics of metakaolin-based geopolymer pastes and mortars. Construction and Building Materials 153(Supplement C), 284-293.

Zhang, M., Guo, H., El-Korchi, T., Zhang, G., Tao, M., 2013. Experimental feasibility study of geopolymer as the next-generation soil stabilizer. Construction and Building Materials 47, 1468-1478.

List of Tables

List of Figures

Table. 1 Chemical composition of basalt rock fines and ground granulated blast furnace slag

Component	**Basalt fines (mass %)**	**GGBFS (mass %)**
SiO_2	51.15	34.46
Al_2O_3	15.89	12.78
CaO	7.00	42.71
Fe_2O_3	8.37	0.39
Na_2O	3.36	0.75
MgO	2.79	5.32
P_2O_5	0.73	0.08
SO_3	0.11	1.68
K_2O	3.71	0.27
Mn_2O_3	0.18	0.39
TiO_2	1.00	0.82
Loss on Ignition (LOI)	5.42	0.14

Table 2. Summary of test matrix for geopolymer preparation

Molarity of NaOH (M)	**Na_2SiO_3/NaOH (R) by mass**	**GGBFS percentage (%) by mass**	**No. of Specimens**
4	0.25	10	3
		20	3
		30	3
	0.5	10	3
		20	3
		30	3
	0.75	10	3
		20	3
		30	3
8	0.25	10	3
		20	3
		30	3
	0.5	10	3
		20	3
		30	3
	0.75	10	3
		20	3
		30	3
12	0.25	10	3
		20	3
		30	3
	0.5	10	3
		20	3
		30	3
	0.75	10	3
		20	3
		30	3
			Total: 81

Table 3. Nash-Sutcliffe Efficiency Index (E_f) values for the proposed model against all confinement pressures

Confinement levels (MPa)	**E_f**
0.2	0.989
0.4	0.990
0.6	0.989
0.8	0.988
1	0.986
2	0.974
3	0.977
4	0.985
5	0.990

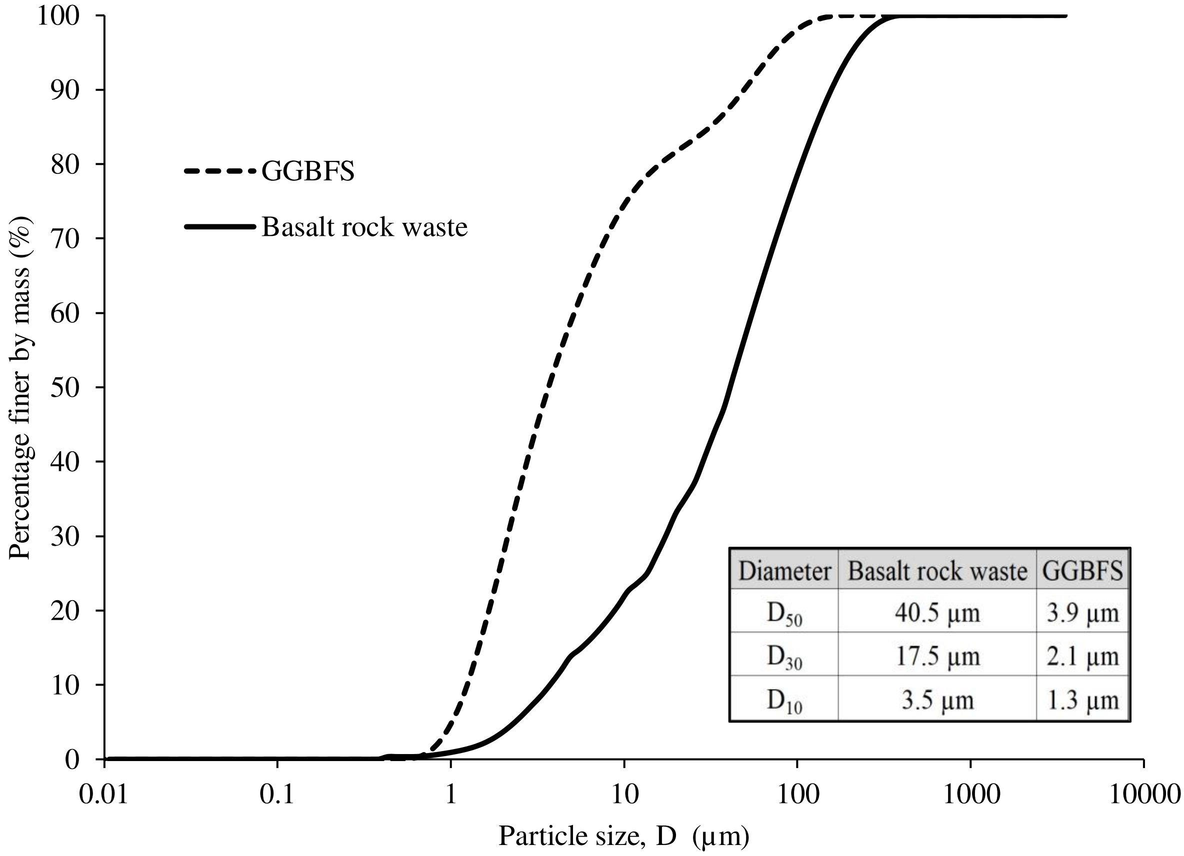

Diameter	Basalt rock waste	GGBFS
D_{50}	40.5 µm	3.9 µm
D_{30}	17.5 µm	2.1 µm
D_{10}	3.5 µm	1.3 µm

Figure 1 Particle size distribution of basalt rock waste and ground granulated blast furnace slag (GGBFS)

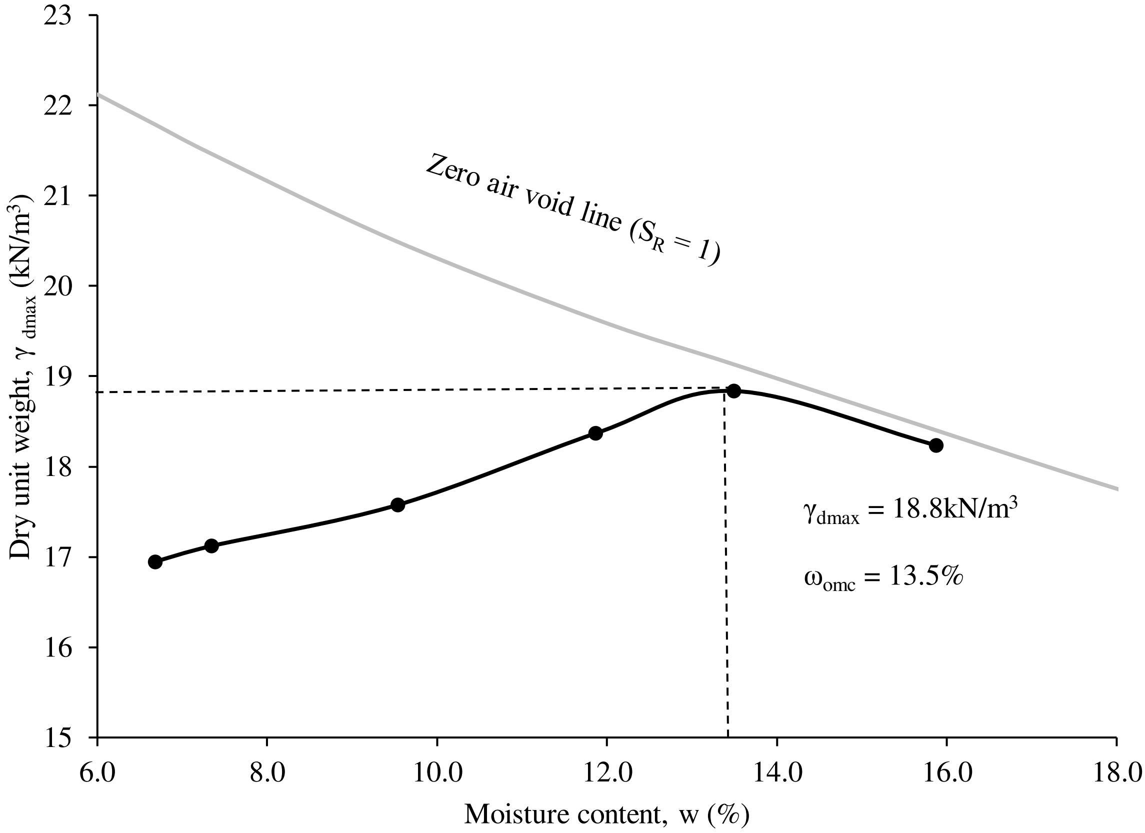

Figure 2 Compaction curve for basalt rock waste

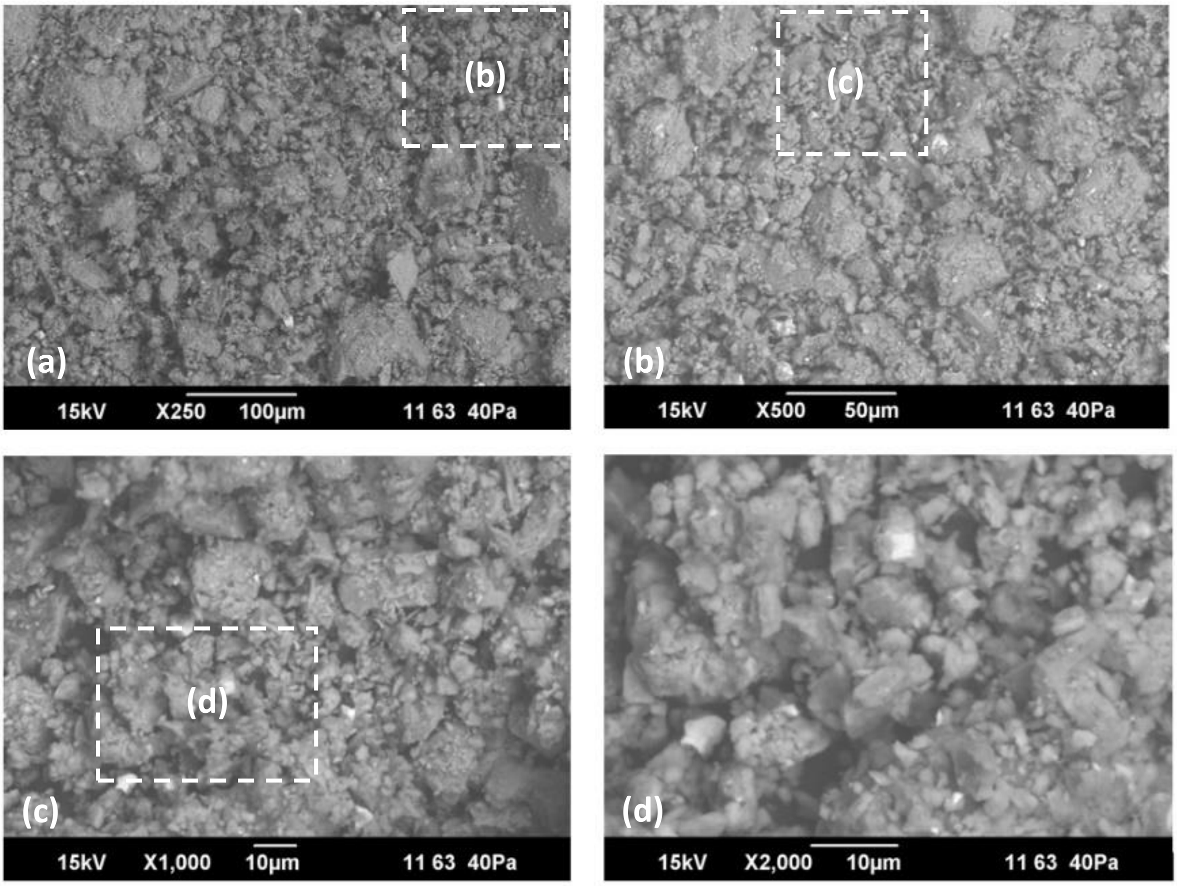

Figure 3 SEM images of basalt fines at various magnifications (a) x250 (b) x500 (c) x1000 and (d) x2000 (Micrographs taken by Mohsin Nawaz) (squares represent the magnified regions)

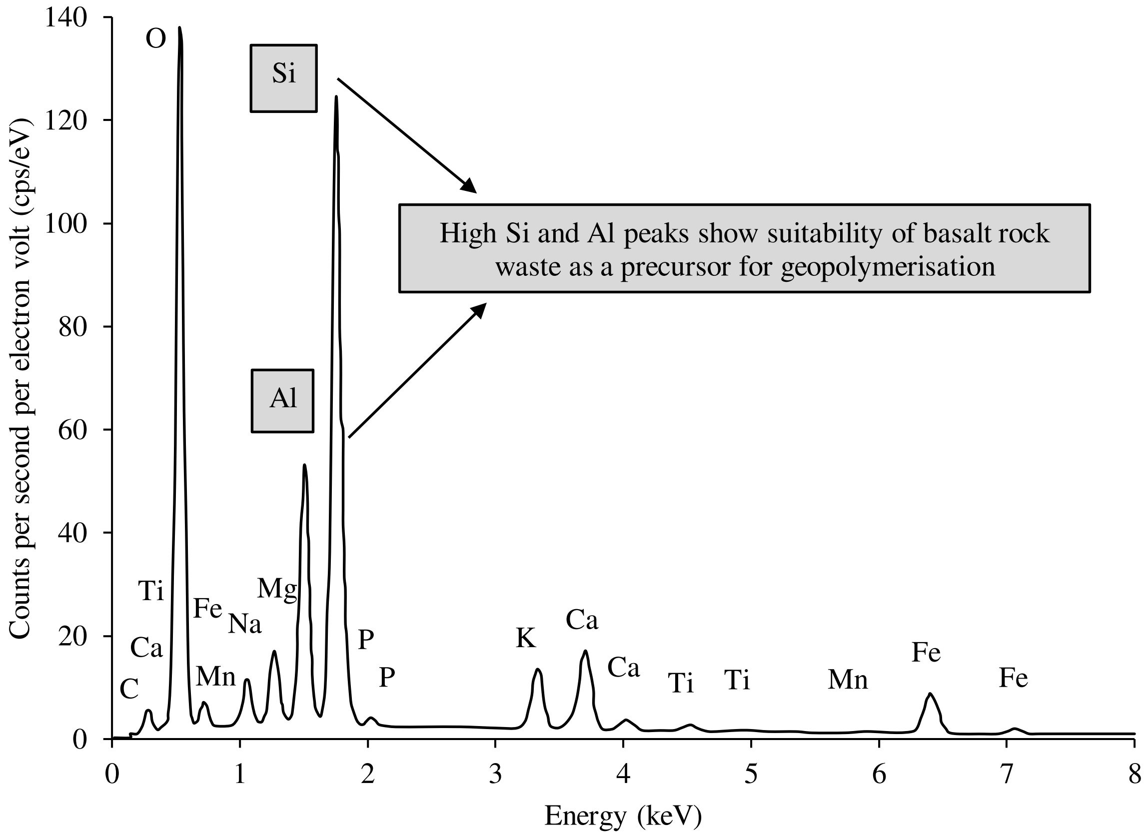

Figure 4 Energy dispersive spectroscopy analysis of basalt rock waste (average spectrum)

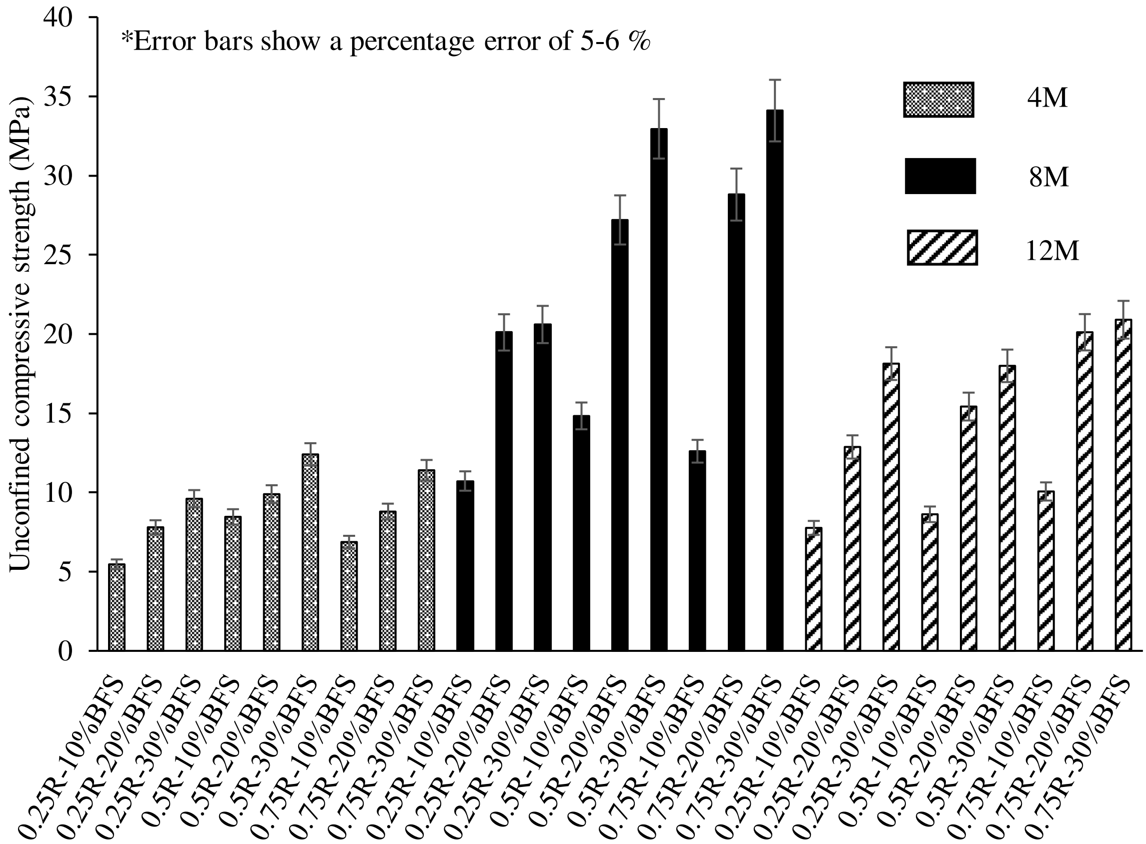

Figure 5 Comparison chart of unconfined compressive strength of basalt rock waste and ground granulated blast furnace slag geopolymer samples

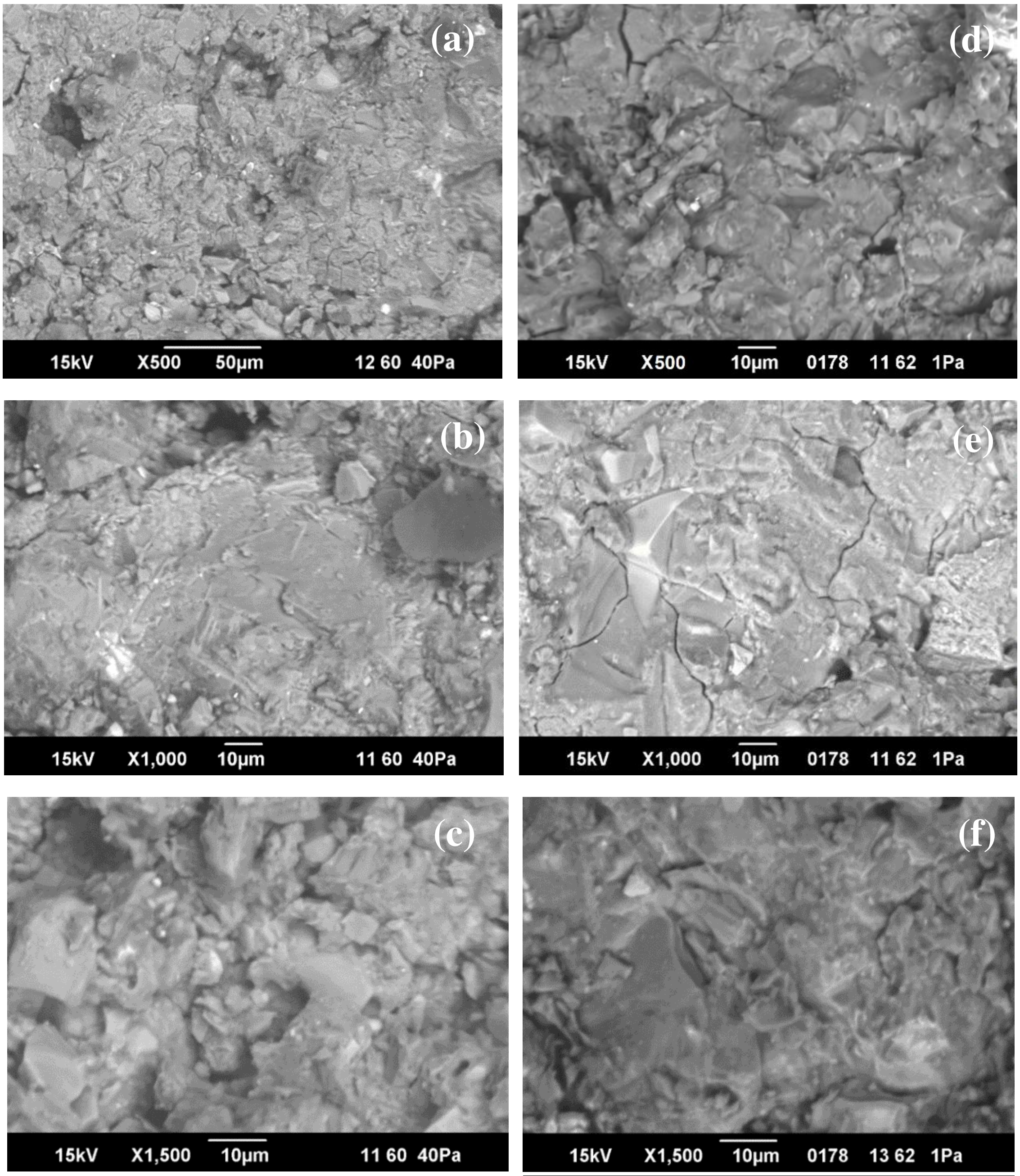

Figure 6 Microstructure of basalt rock waste and blast furnace slag geopolymer (8M-0.75R-30%BFS) after 7 days (a) x500 (b) x1000 (c) x1500 and 28 days (d) x500 (e) x1000 and (f) x1500 (Micrographs taken by Mohsin Nawaz)

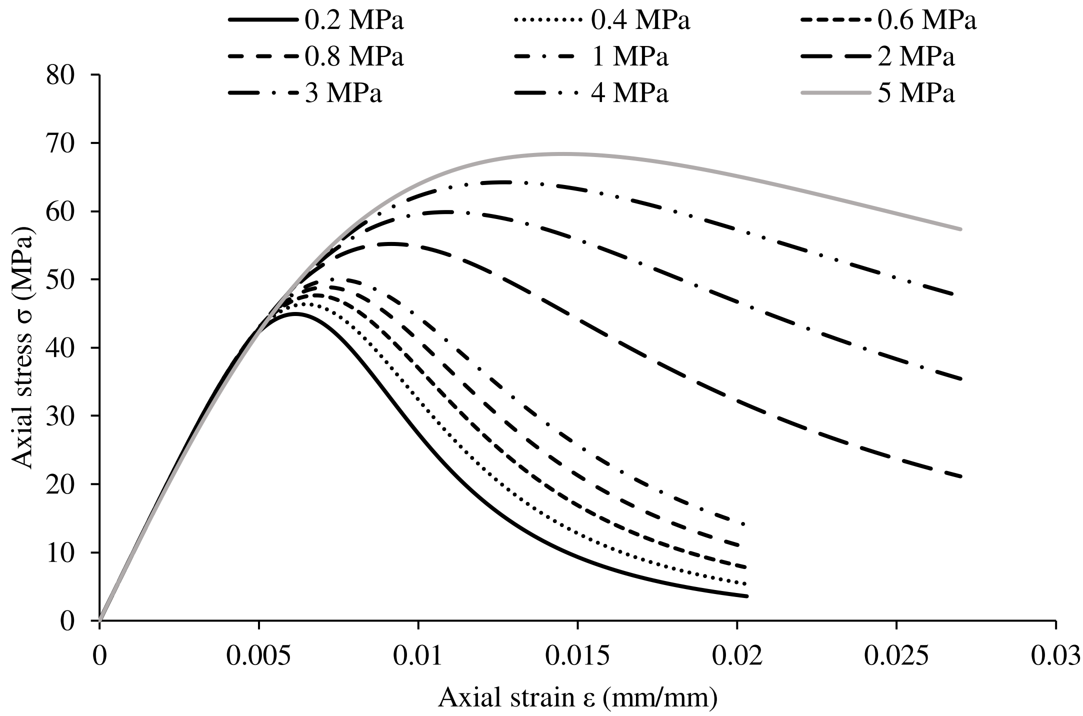

Figure 7 Stress-strain curves for geopolymer samples under varying levels of confinement

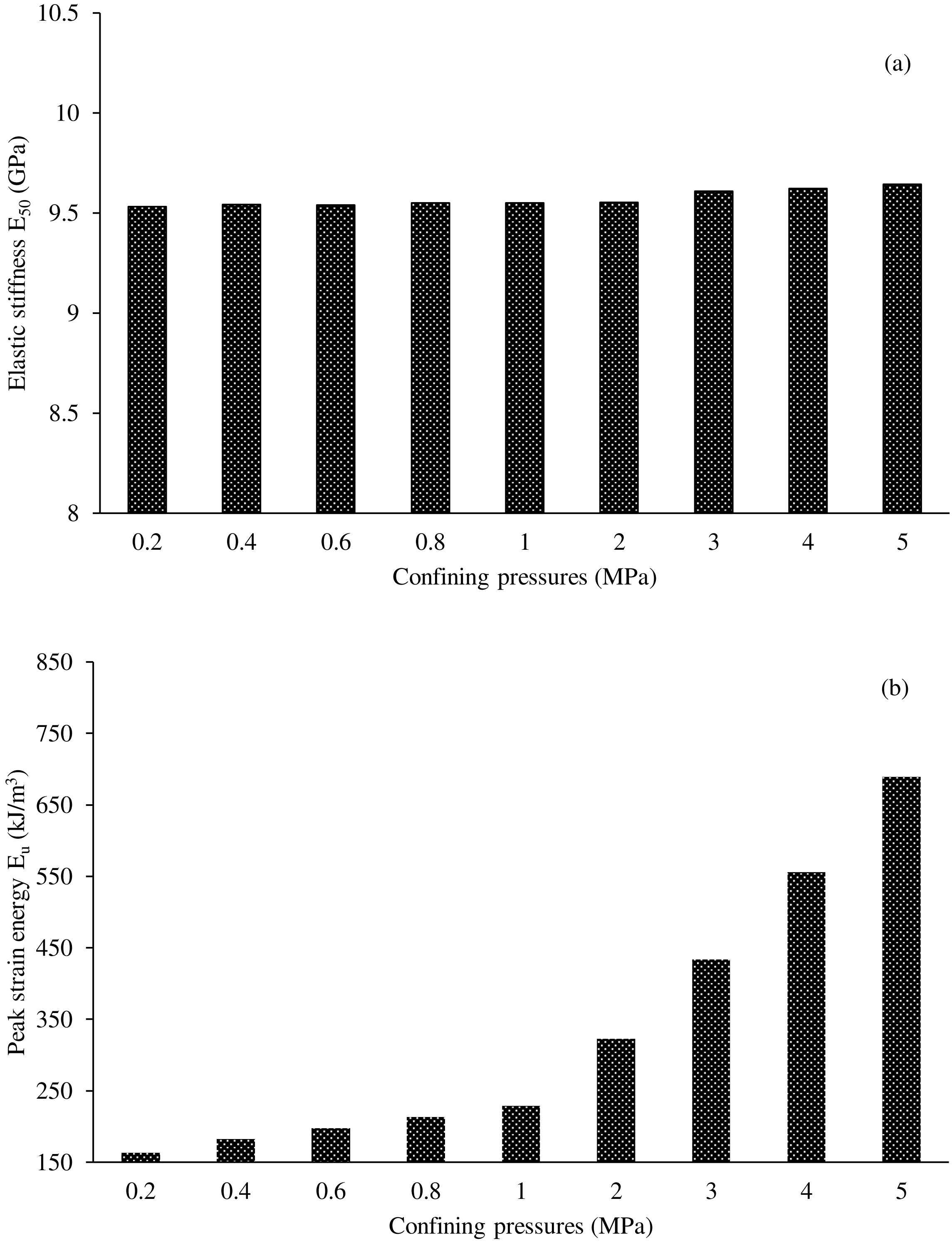

Figure 8 Effect of confining pressures on (a) Elastic stiffness of geopolymer (E_{50}) and (b) Peak strain energy (E_u) of geopolymer

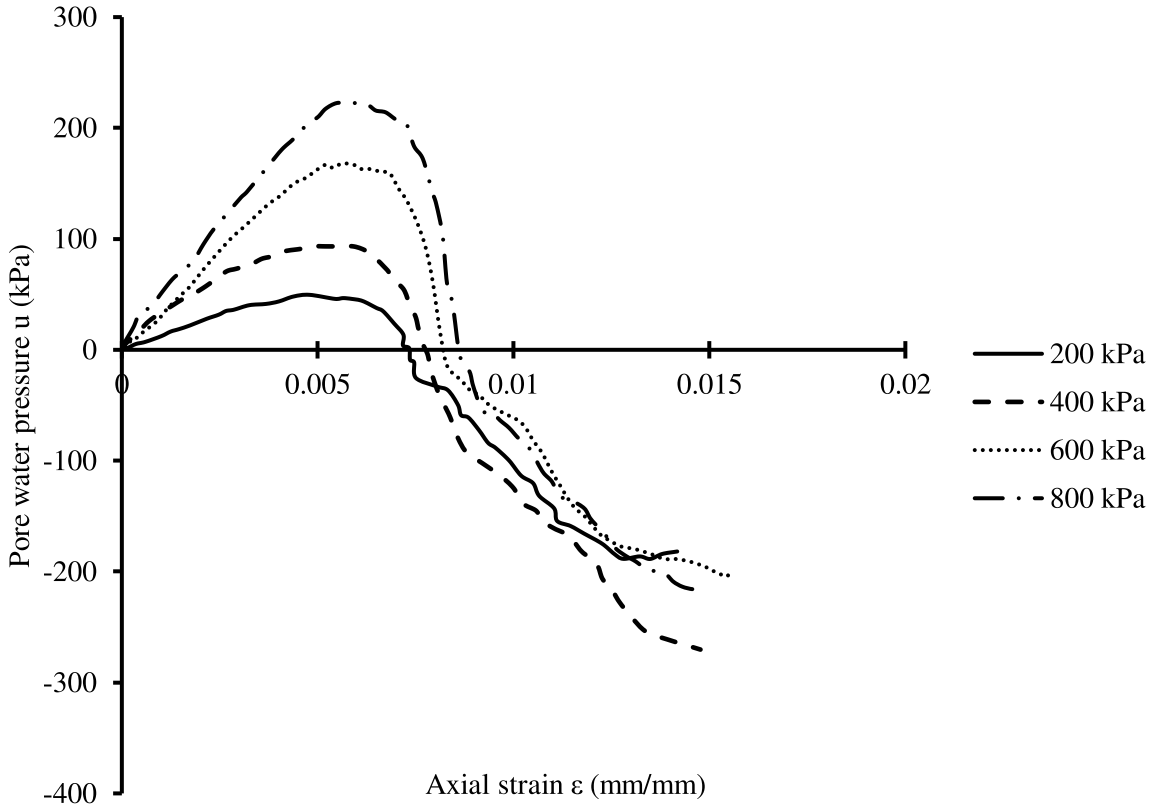

Figure 9 Pore pressure curves for geopolymer specimens tested under low confining pressures

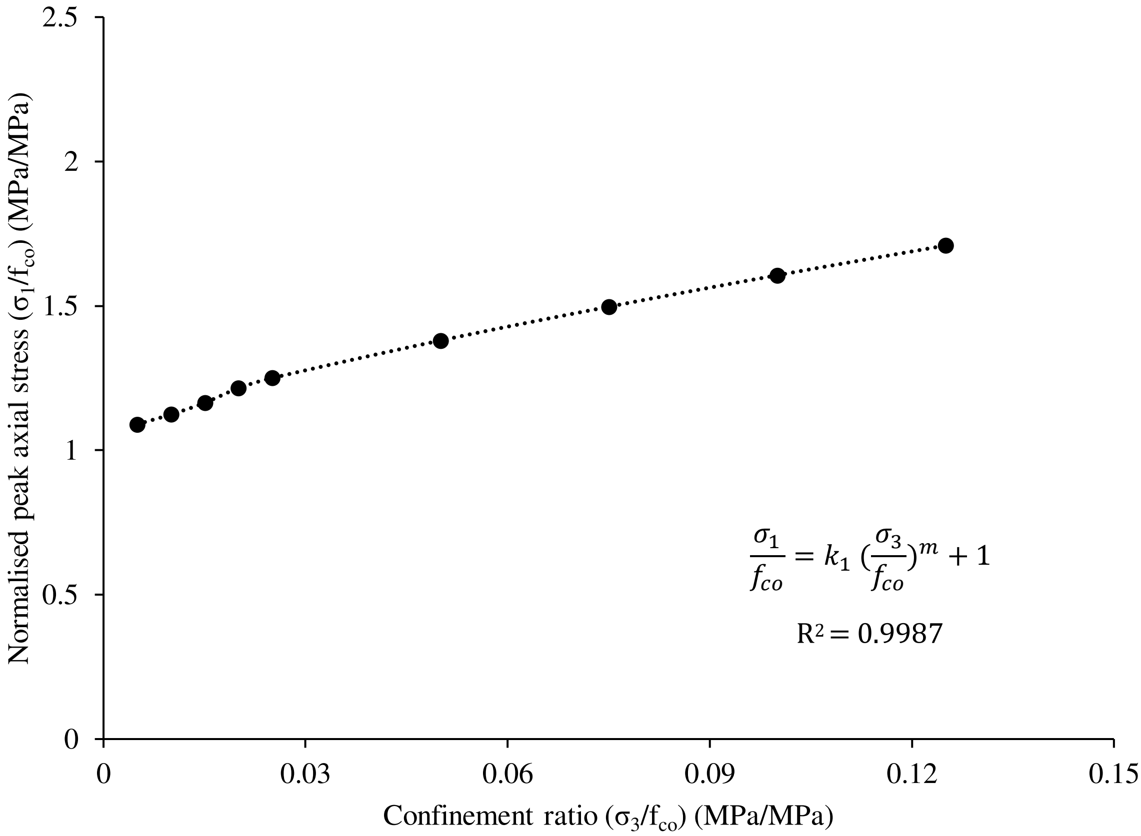

Figure 10 Normalised axial stress versus confinement ratio for geopolymer

($k_1 = 2.89$ and $m = 0.68$)

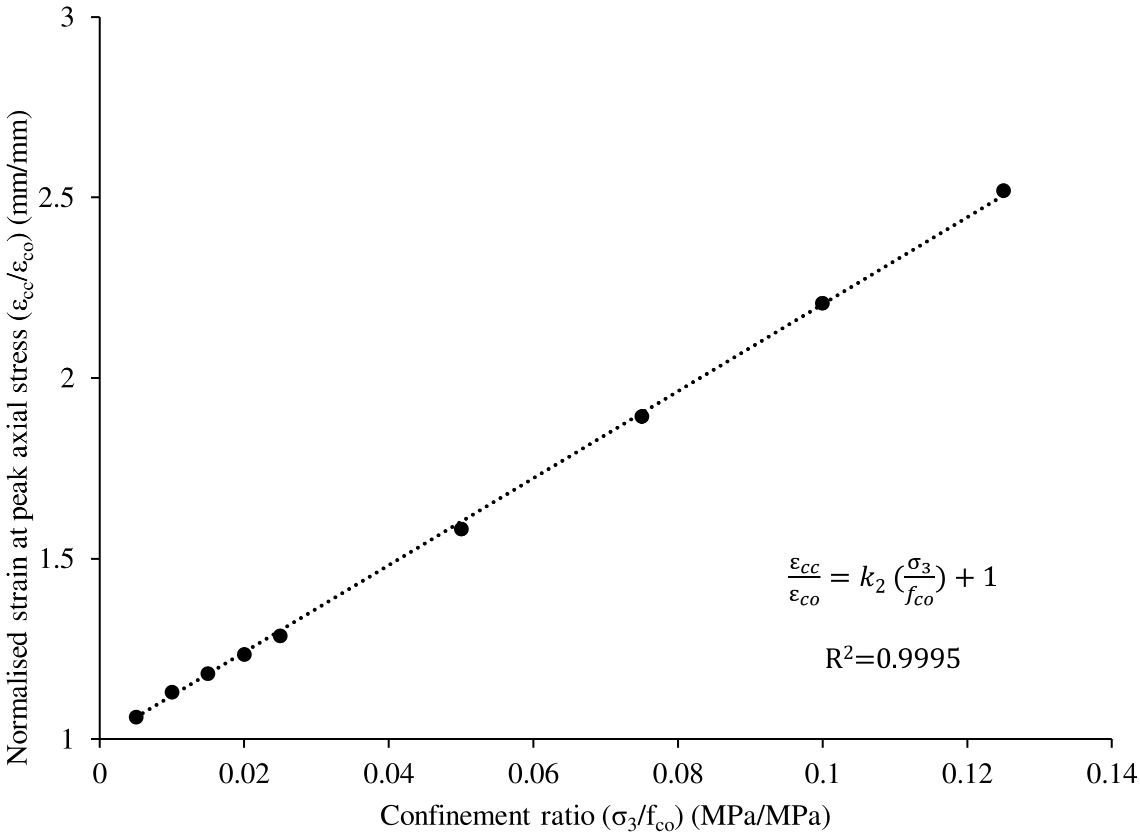

Figure 11 Normalised axial strain versus confinement ratio for geopolymer (k_2 =12.04)

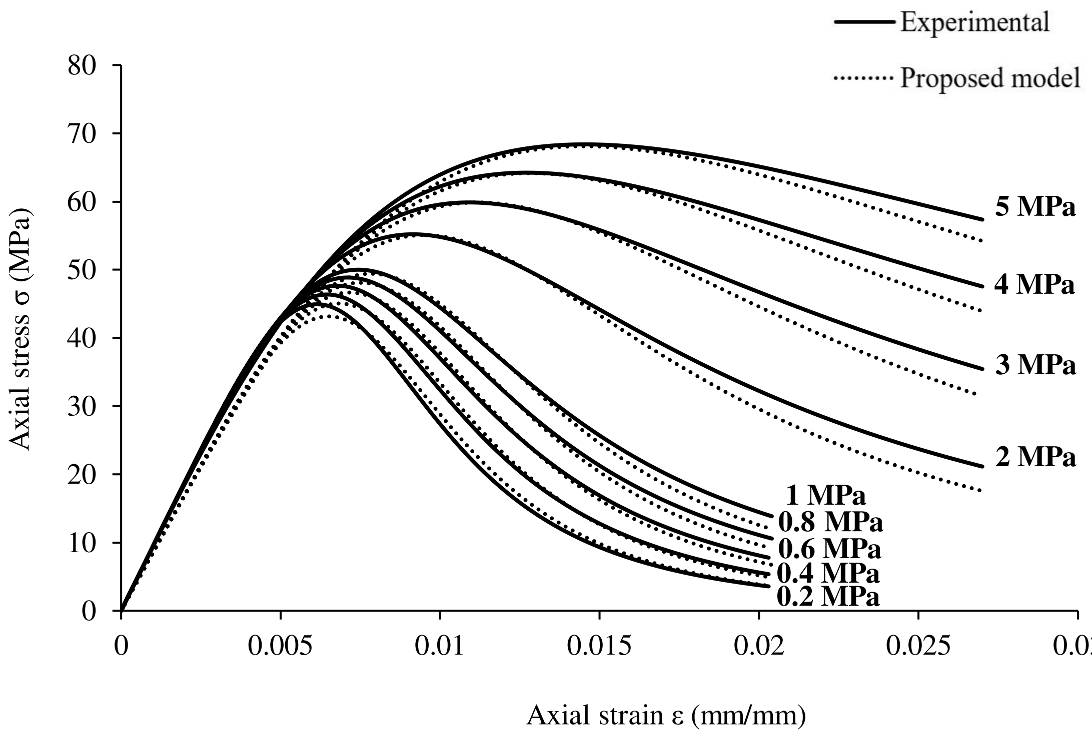

Figure 12 Experimental and proposed model stress-strain curves for geopolymer specimens

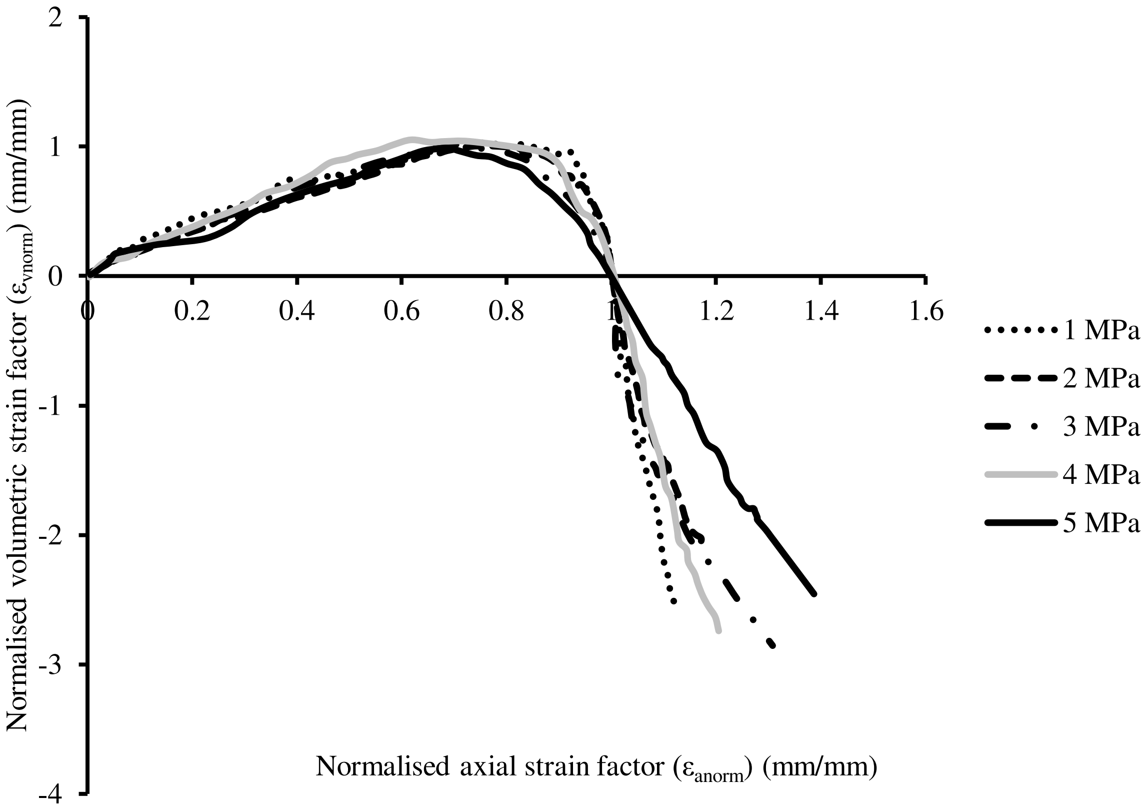

Figure 13 Normalised volumetric strain factor versus normalised axial strain factor for geopolymer

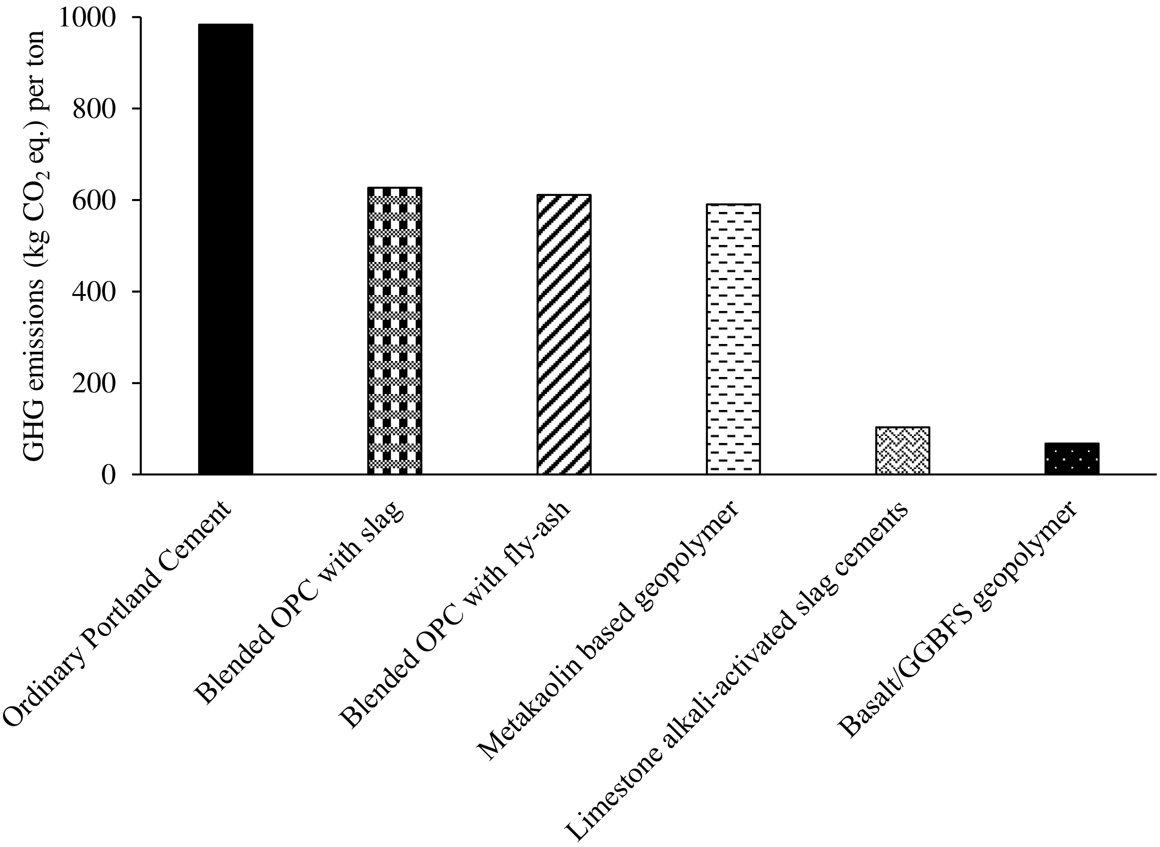

Figure 14 Comparison of greenhouse gas emissions of basalt rock waste and GGBFS geopolymer with other cementitious binders